URSI GASS 2023, Sapporo, Japan, 19 – 26 August 2023

Solving Combined Field Integral Equations of 3D PEC Targets Based on Physics-informed Graph Residual Learning

Tao Shan(1), Maokun Li*(1), Fan Yang(1) and Shenheng Xu(1)
(1) Beijing National Research Center for Information Science and Technology (BNRist), Department of Electronic Engineering, Tsinghua University, Beijing, China; e-mail: maokunli@tsinghua.edu.cn

Abstract

In this paper, we present physics-informed graph residual learning (PhiGRL) to model the scattering of 3D PEC targets by solving combined field integral equations (CFIEs). Emulating the computing process of the fixed-point iteration method, PhiGRL iteratively modifies the candidate solutions of CFIEs regarding the residuals of CFIEs until convergence. In each iteration, the matrix-vector multiplication of CFIE is incorporated to guide PhiGRL. The graph neural networks (GNNs) are applied to deal with the unstructured discretization and varying unknown numbers. With the data set generated by the method of moments (MoM), PhiGRL is first trained to model the scattering of basic 3D PEC targets, including spheroids, conical frustums, and hexahedrons. Furthermore, the transfer learning strategy is adopted to migrate PhiGRL to simulate airplane-shaped targets. Numerical results validate that PhiGRL can provide real-time and accurate simulations of 3D PEC targets. This study explores the feasibility of combining deep learning and physics to accelerate the 3D EM modeling.

1 Introduction

Electromagnetic (EM) modeling has been widely applied in electronic engineering and scientific research [1, 2]. The aim of EM modeling is to accurately describe electromagnetic phenomenon by applying computational methods to numerically solve Maxwell's equations with certain boundary conditions. Typical computational methods include finite-difference method [3], finite-element method [4] and MoM [5]. In practical applications, especially 3D EM modeling problems, there are usually a large number of unknowns, making the solving process computationally expensive. It still remains challenging to perform real-time simulations in 3D EM modeling.

Recently, with the development of high-performance computing, artificial intelligence, especially deep learning (DL), has been applied in EM modeling, demonstrating unprecedented computational efficiency [6–14]. Deep neural networks (DNNs) can be trained directly to approximate the nonlinear mappings between different physical quantities [9–12]. These models can improve the computational efficiency with the help of massive parallelization [9–12]. However, they have poor interpretability and their performances are highly dependent on data quality. To overcome these drawbacks, EM physics and numerical methods are further incorporated into DNNs for improved robustness and interpretability [13, 14]. Despite the successful application of DL, the solved problems are mostly based on uniform discretization. This is limited by the fact that the applied DL techniques are designed for structured data. In 3D EM modeling, unstructured grids are usually adopted, such as triangular or tetrahedral meshes, which makes most DL techniques inapplicable. The issue of applying DL to 3D EM modeling defined on nonuniform grids still needs to be addressed.

In this paper, we present physics-informed graph residual learning to model the scattering of 3D PEC targets by solving combined field integral equations. PhiGRL emulates the computation of the fixed-point iteration method and iteratively modifies the candidate solutions of CFIEs until convergence. In each iteration of PhiGRL, the residuals of CFIEs are first numerically calculated by incorporating the matrix-vector multiplications of CFIEs. Then, the residuals are input to GNNs for predicting modifications of candidate solutions, which guides the training of PhiGRL. The applied GNNs can flexibly tackle the triangular meshes of 3D PEC targets in the form of a graph data structure. PhiGRL is first applied to model basic 3D PEC targets, including spheroids, conical frustums, and hexahedrons. Furthermore, transfer learning is adopted to migrate PhiGRL for objects with complex structures, including three types of airplane-shaped targets. The required data sets for training PhiGRL are generated by MoM. Numerical results validate that PhiGRL can accurately model 3D PEC targets with different meshes in real time.

2 Formulation

The surface current of a 3D PEC target satisfies CFIE, which is a weighted combination of electric-field integral equation (EFIE) and magnetic-field integral equation (MFIE) [1, 2]:

$$\begin{aligned} &\text{CFIE} = (1-\alpha)\cdot\text{MFIE} - \alpha\cdot\hat{n}\times\text{EFIE} \\ &\text{EFIE: } \hat{n}\times\overline{\overline{\mathscr{L}}}\left(\overline{\mathbf{J}}_\text{s}\right) = \hat{n}\times\mathbf{E}^\text{inc}(\mathbf{r}),\ \mathbf{r}\in S_\text{o} \\ &\text{MFIE: } \frac{1}{2}\overline{\mathbf{J}}_\text{s} + \hat{n}\times\overline{\overline{\mathscr{K}}}\left(\overline{\mathbf{J}}_\text{s}\right) = \hat{n}\times\overline{\mathbf{H}}^\text{inc}(\mathbf{r}),\ \mathbf{r}\in S_\text{o} \end{aligned} \tag{1}$$

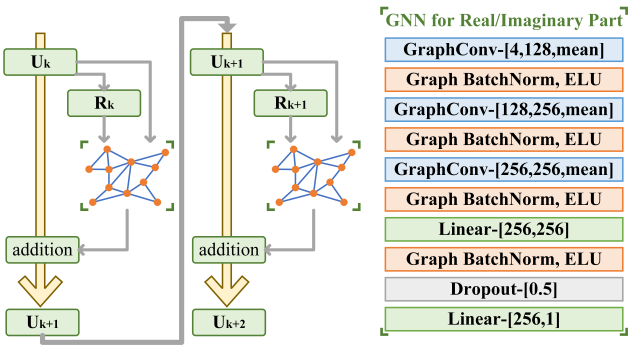

Figure 1. Structure of PhiGRL. GraphConv-[a, b, mean] denotes the graph convolutional layer of which the input channel, output channel, and aggregation function are a, b, mean function. Linear-[c,d] denotes the input and output channel of the linear layer are c and d. Dropout-[0.5] denotes that the dropout rate of the linear layer is 0.5.

where S_o and $\hat{n}$ are the target surface and its normal vector, $\mathbf{E}^{\text{inc}}$, $\mathbf{H}^{\text{inc}}$ and $\mathbf{J}_s$ are incident electric, magnetic field and surface current, $\overline{\mathbf{J}}_s = Z_0\mathbf{J}_s$ and $\overline{\mathbf{H}}^{\text{inc}}(\mathbf{r}) = Z_0\mathbf{H}^{\text{inc}}(\mathbf{r})$, Z_0 is the wave impedance, $\alpha = 0.5$. The definitions of $\overline{\overline{\mathscr{L}}}$ and $\overline{\overline{\mathscr{K}}}$ can refer to [1, 2]. By applying MoM and Rao–Wilton–Glisson (RWG) basis functions, CFIE can be discretized into a matrix equation:

$$\mathbb{Z}\cdot\mathbf{u} = \mathbf{b} \tag{2}$$

where $\mathbb{Z}$, $\mathbf{u}$ and $\mathbf{b}$ denote the impedance matrix, unknowns and excitation vector.

Drawing on the fixed-point iteration method, the k-th update equation of PhiGRL to solve Eq. (2) can be written as [14]:

$$\begin{aligned}
\mathbf{u}_{k+1} &= \mathbf{u}_k^r + \Delta_k^r + j(\mathbf{u}_k^i + \Delta_k^i)\\
\Delta_k^r &= \Psi^r(\mathbf{R}_k \oplus \mathbf{u}_k, \Theta^r)\\
\Delta_k^i &= \Psi^i(\mathbf{R}_k \oplus \mathbf{u}_k, \Theta^i)\\
\mathbf{R}_k &= \mathbf{b} - \mathbb{Z}\mathbf{u}_k
\end{aligned} \tag{3}$$

where $\oplus$ denotes the tensor concatenation, Ψ^r and Ψ^i are GNNs to update the real and imaginary part and they are parameterized by Θ^r and Θ^i respectively. Ψ^r and Ψ^i have the same structure but different parameter sets, as shown in Figure 1. They comprise graph convolution, graph batch normalization, ELU nonlinearity, and linear transformation.

In order to apply GNNs, the RWG functions need to be described in a graph data structure. A graph can be represented by a pair of two sets (V,E). $V = \{v_1,\cdots,v_N\}$ is a finite set of N nodes and $E = \{e_{ij} | e_{ij} = (v_i, v_j) \subseteq V^2, v_i \neq v_j\}$ is a set of edges. Then, the graph convolution can be applied, which is expressed as [15]:

$$f_{l+1}(v_{l+1}^i) = \mathbf{W}_s f_l(v_l^i) + \mathbf{W}_a \frac{1}{N_{\mathscr{N}(i)}} \sum_{j\in\mathscr{N}(i)} e_{j,i}\cdot f_l(v_l^j)\,, \tag{4}$$

where $f_l(v_l^i)$ is the feature map of the i-th node at the l-th layer, $\mathscr{N}(i)$ is the index set of adjacent nodes of v_l^i, $N_{\mathscr{N}(i)}$ is the number of adjacent nodes in $\mathscr{N}(i)$, $e_{j,i}$ is the edge between v_l^j and v_l^i, $\mathbf{W}_s$ and $\mathbf{W}_a$ are trainable parameters of v_l^i itself and its adjacent nodes. The contributions from adjacent nodes are averaged in Eq. (4), which is named mean aggregation.

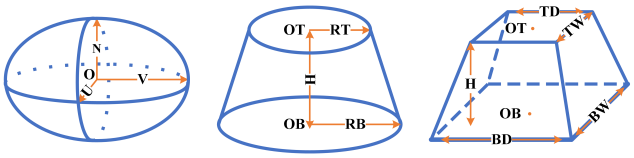

Figure 2. Illustration of basic 3D PEC targets. O, OT and OB denote the body, top, and base center.

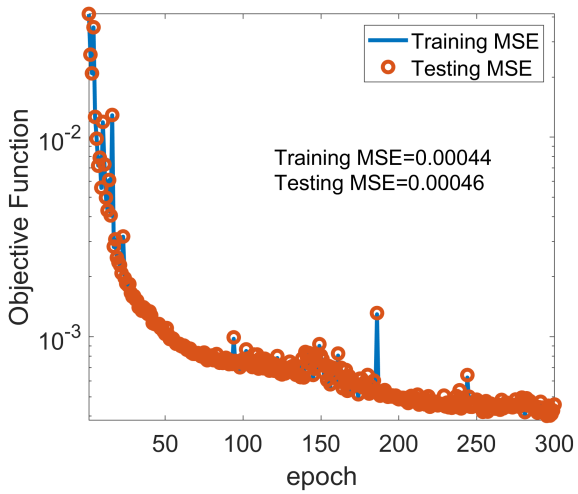

Figure 3. MSE convergence curve of PhiGRL. The values of MSE at the 300th epoch are also annotated.

The supervised learning scheme is adopted to train PhiGRL. With the surface currents computed by MoM as ground truth, mean squared error (MSE) is applied as the objective function:

$$\text{MSE} = \frac{||\mathbf{u}_m^r - \mathbf{u}_g^r||_2^2}{N_{\mathbf{u}_m}} + \frac{||\mathbf{u}_m^i - \mathbf{u}_g^i||_2^2}{N_{\mathbf{u}_m}}\,, \tag{5}$$

where $\mathbf{u}_m$ and $\mathbf{u}_g$ denote the RWG coefficients computed by MoM and PhiGRL, $N_{\mathbf{u}_m}$ is the element number of $\mathbf{u}_m$.

3 Numerical Example

The effectiveness of PhiGRL is first verified by solving CFIEs of basic 3D PEC targets. PhiGRL is assumed to have 7 iterations. The illuminating wave is vertically polarized with the amplitude and frequency of 1 and 300 MHz. The incident angle θ and ϕ vary in $[10°, 90°]$ and $[90°, 180°]$ in a step of $10°$. Three types of basic 3D PEC targets are taken into account, including spheroids, conical frustums, and hexahedrons, as shown in Figure 2. Their body centers are located at the coordinate origin. The corresponding geometrical parameters vary from 0.2 to 0.7m and they are different from each other. Figure 3 plots the MSE convergence curve of PhiGRL. During the training process, both

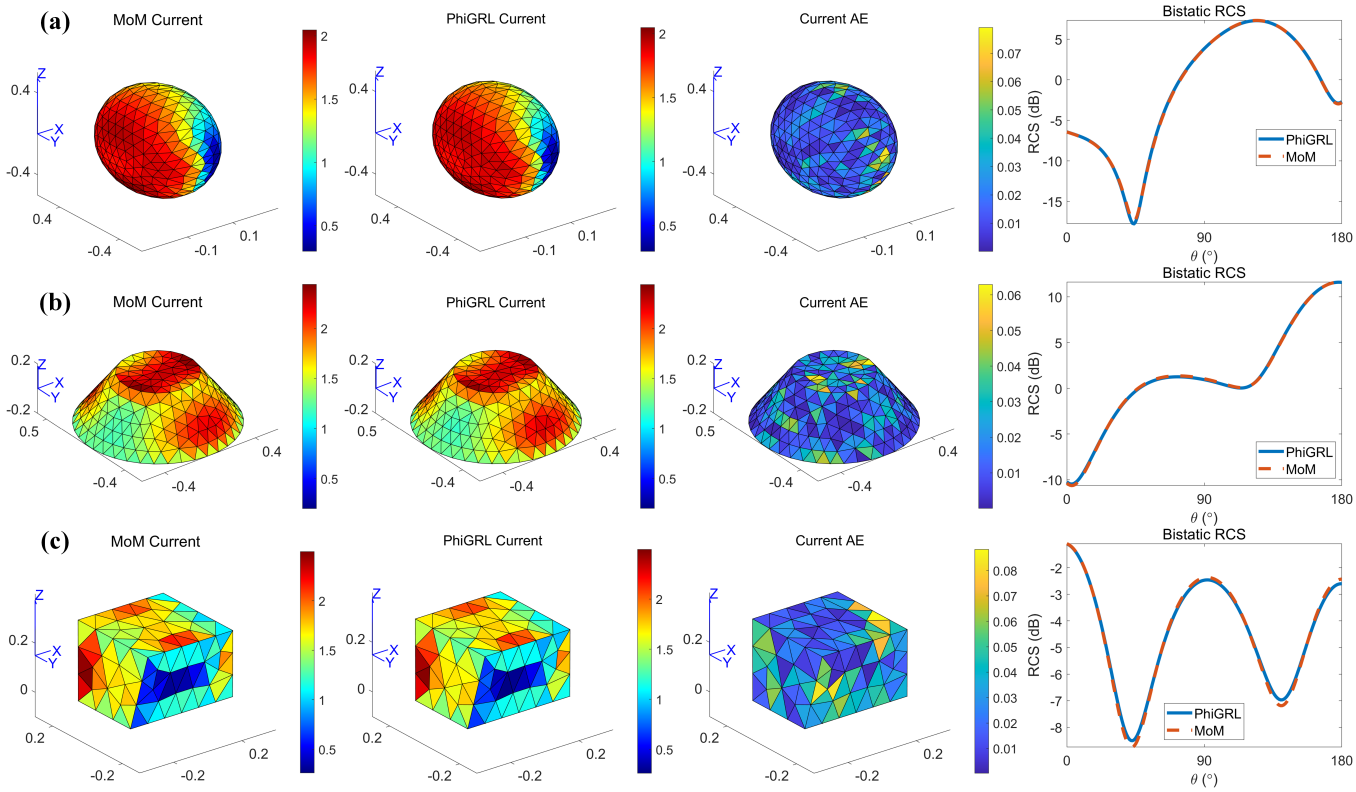

Figure 4. Comparison between the surface currents computed by MoM and PhiGRL. In each panel, from left to right are: 3D surface currents computed by MoM and PhiGRL, absolute error (AE) distribution, bistatic RCS curves on the $\phi = 0^\circ$ plane.

training and testing MSE drop steadily and they agree well with each other, which indicates little overfitting. The average length of the triangular mesh is $\frac{\lambda}{10}$ where λ denotes wavelength. MoM generates 32400 data samples that are divided for training and testing by 80%-20% ratio. Figure 4 demonstrates three comparisons between the surface currents computed by MoM and PhiGRL. It can be observed that not only the predicted and true 3D surface currents are in good agreement, but also the corresponding bistatic radar cross-section (RCS) curves on the $\phi = 0^\circ$ plane match well.

Furthermore, PhiGRL is applied to model objects with complex structures in a transfer learning manner. Three types of airplane-shaped targets are considered here, including plane A, B, and C, as shown in Figure 5. The corresponding control parameters are also denoted in Figure 5. Transfer learning allows the migration of learned knowledge between analogous domains, which further reduces training difficulty and the amount of data for a new knowledge domain [16]. PhiGRL is assumed to have 11 iterations, according to the author's trials, because the structures of airplane-shaped targets are complex. The PhiGRL model trained for basic 3D PEC targets is taken as an initialization of the first 7 iterations here. The frequency and amplitude of the vertically polarized illuminating wave are 150 MHz and 0.5. The incident angle θ and ϕ vary in $[0^\circ, 180^\circ]$ and $[3^\circ, 180^\circ]$ with a step of 5° and 3° respectively. The average length of the triangular mesh is set as $\frac{\lambda}{10}$. 6660 data samples are generated by MoM, and they are divided for

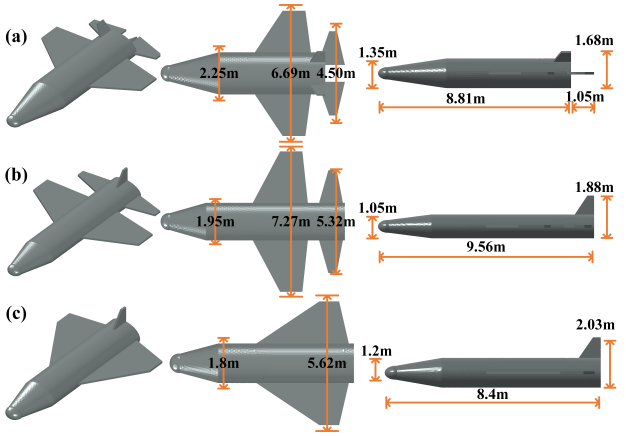

Figure 5. Illustration of airplane-shaped targets. (a), (b) and (c) are plane A, plane B and plane C respectively.

training and testing based on 80%-20% ratio. The final MSE of PhiGRL converges below 0.0052. Figure 6 compares the surface currents computed by MoM and PhiGRL. The predictions are in good agreement with ground truth and the errors between the corresponding RCS curves are also small.

4 Conclusions

In this study, we present PhiGRL to model the scattering of 3D PEC targets by solving CFIEs. PhiGRL iteratively

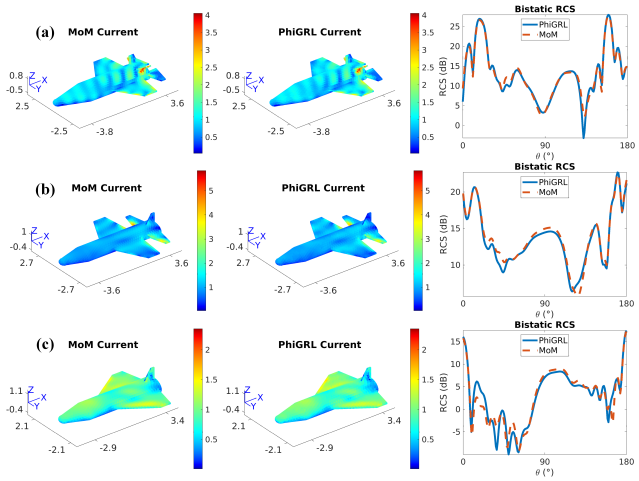

Figure 6. The surface currents of airplane-shaped targets. In each panel, from left to right are: 3D surface currents computed by MoM and PhiGRL, their AE distribution, bistatic RCS curves on the $\phi = 0^\circ$ plane.

modifies candidate solutions until convergence by applying GNNs to predict modifications. During iteration, the matrix-vector multiplications of CFIEs are incorporated to provide physical information. PhiGRL is first to model basic 3D PEC targets, including spheroids, conical frustums, and hexahedrons. Then, PhiGRL is migrated for objects with complex structures, including three types of airplane-shaped targets. Numerical results validate that PhiGRL can provide real-time and accurate simulations of various 3D PEC targets with different unknown numbers. This study offers a potential way to combine graph neural networks and electromagnetic physics for 3D EM modeling with nonuniform discretization.

Acknowledgements

This work was supported in part by the China Postdoctoral Science Foundation under Grant 2022M711764, the National Natural Science Foundation of China under Grant 61971263, the Institute for Precision Medicine, Tsinghua University, the Biren Technology, and the BGP Inc.

References

[1] W. C. Chew, E. Michielssen, J. Song, and J.-M. Jin, *Fast and efficient algorithms in computational electromagnetics*. Artech House, Inc., 2001.

[2] J.-M. Jin, *Theory and computation of electromagnetic fields*. John Wiley & Sons, 2011.

[3] A. Taflove, S. C. Hagness, and M. Piket-May, "Computational electromagnetics: the finite-difference time-domain method," *The Electrical Engineering Handbook*, vol. 3, pp. 629–670, 2005.

[4] J.-M. Jin, *The finite element method in electromagnetics*. John Wiley & Sons, 2015.

[5] R. F. Harrington and J. L. Harrington, *Field computation by moment methods*. Oxford University Press, Inc., 1996.

[6] Y. LeCun, Y. Bengio, and G. Hinton, "Deep learning," *nature*, vol. 521, no. 7553, pp. 436–444, 2015.

[7] A. Massa, D. Marcantonio, X. Chen, M. Li, and M. Salucci, "Dnns as applied to electromagnetics, antennas, and propagation—a review," *IEEE Antennas and Wireless Propagation Letters*, vol. 18, no. 11, pp. 2225–2229, 2019.

[8] M. Salucci, M. Arrebola, T. Shan, and M. Li, "Artificial intelligence: New frontiers in real–time inverse scattering and electromagnetic imaging," *IEEE Transactions on Antennas and Propagation*, 2022.

[9] T. Shan, W. Tang, X. Dang, M. Li, F. Yang, S. Xu, and J. Wu, "Study on a fast solver for poisson's equation based on deep learning technique," *IEEE Transactions on Antennas and Propagation*, vol. 68, no. 9, pp. 6725–6733, 2020.

[10] T. Shan, R. Guo, M. Li, F. Yang, S. Xu, and L. Liang, "Application of multitask learning for 2-d modeling of magnetotelluric surveys: Te case," *IEEE Transactions on Geoscience and Remote Sensing*, vol. 60, pp. 1–9, 2021.

[11] H. M. Yao and L. Jiang, "Machine-learning-based pml for the fdtd method," *IEEE Antennas and Wireless Propagation Letters*, vol. 18, no. 1, pp. 192–196, 2018.

[12] J.-J. Sun, S. Sun, Y. P. Chen, L. Jiang, and J. Hu, "Machine-learning-based hybrid method for the multilevel fast multipole algorithm," *IEEE Antennas and Wireless Propagation Letters*, vol. 19, no. 12, pp. 2177–2181, 2020.

[13] Y. Hu, Y. Jin, X. Wu, and J. Chen, "A theory-guided deep neural network for time domain electromagnetic simulation and inversion using a differentiable programming platform," *IEEE Transactions on Antennas and Propagation*, vol. 70, no. 1, pp. 767–772, 2021.

[14] T. Shan, X. Song, R. Guo, M. Li, F. Yang, and S. Xu, "Physics-informed supervised residual learning for 2d electromagnetic forward modeling," *arXiv preprint arXiv:2104.13231*, 2021.

[15] C. Morris, M. Ritzert, M. Fey, W. L. Hamilton, J. E. Lenssen, G. Rattan, and M. Grohe, "Weisfeiler and leman go neural: Higher-order graph neural networks," in *Proceedings of the AAAI conference on artificial intelligence*, vol. 33, no. 01, 2019, pp. 4602–4609.

[16] F. Zhuang, Z. Qi, K. Duan, D. Xi, Y. Zhu, H. Zhu, H. Xiong, and Q. He, "A comprehensive survey on transfer learning," *Proceedings of the IEEE*, vol. 109, no. 1, pp. 43–76, 2020.